Conformation of Alamethicin in Oriented Phospholipid Bilayers Determined by ^{15}N Solid-State Nuclear Magnetic Resonance

Mads Bak,* Robert P. Bywater,† Morten Hohwy,* Jens K. Thomsen,* Kim Adelhorst,† Hans J. Jakobsen,‡ Ole W. Sørensen,§ and Niels C. Nielsen*

*Laboratory for Biomolecular NMR Spectroscopy, Department of Molecular and Structural Biology, Science Park, University of Aarhus, DK-8000 Aarhus C, †Biostructure Department, Novo Nordisk A/S, Novo Nordisk Park, DK-2760 Måløv, ‡Instrument Centre for Solid-State NMR Spectroscopy, Department of Chemistry, University of Aarhus, DK-8000 Aarhus C, and §Department of Chemistry, Carlsberg Laboratory, DK-2500 Valby, Denmark

ABSTRACT The conformation of the 20-residue antibiotic ionophore alamethicin in macroscopically oriented phospholipid bilayers has been studied using ^{15}N solid-state nuclear magnetic resonance (NMR) spectroscopy in combination with molecular modeling and molecular dynamics simulations. Differently ^{15}N-labeled variants of alamethicin and an analog with three of the α-amino-isobutyric acid residues replaced by alanines have been investigated to establish experimental structural constraints and determine the orientation of alamethicin in hydrated phospholipid (dimyristoylphosphatidylcholine) bilayers and to investigate the potential for a major kink in the region of the central Pro^{14} residue. From the anisotropic ^{15}N chemical shifts and ^{1}H–^{15}N dipolar couplings determined for alamethicin with ^{15}N-labeling on the Ala^{6}, Val^{9}, and Val^{15} residues and incorporated into phospholipid bilayer with a peptide:lipid molar ratio of 1:8, we deduce that alamethicin has a largely linear α-helical structure spanning the membrane with the molecular axis tilted by 10–20° relative to the bilayer normal. In particular, we find compatibility with a straight α-helix tilted by 17° and a slightly kinked molecular dynamics structure tilted by 11° relative to the bilayer normal. In contrast, the structural constraints derived by solid-state NMR appear not to be compatible with any of several model structures crossing the membrane with vanishing tilt angle or the earlier reported x-ray diffraction structure (Fox and Richards, *Nature.* 300:325–330, 1982). The solid-state NMR-compatible structures may support the formation of a left-handed and parallel multimeric ion channel.

INTRODUCTION

To clarify the mechanisms by which voltage-gated ion channels operate in biological membranes, considerable effort has been devoted to investigation of the structure and function of small peptide ion channels. Numerous synthetic and naturally occurring peptides have been examined using a variety of analytical methods. Among the small natural polypeptides, the amphipathic 20-residue peptaibophol alamethicin is probably the most extensively studied ionophore (Woolley and Wallace, 1993; Sansom, 1993; Cafiso, 1994). The most common form of alamethicin has the amino acid sequence (Pandey et al., 1977) *Ac*-Aib-Pro-Aib-Ala-Aib-Ala-Gln-Aib-Val-Aib-Gly-Leu-Aib-Pro-Val-Aib-Aib-Glu-Gln-*Phol*, where the N-terminal residue is acetylated and the C-terminal residue is L-phenylalaninol. Because of its tractable size and its significant voltage-dependent conductance in lipid bilayer systems, alamethicin has been regarded an ideal model for studying voltage-gated conformational changes in α-helical antibacterial peptides, transmembrane ion transport, and helix–membrane interactions for membrane proteins in more general terms. Due to the presence of a central proline residue within the potentially membrane-buried part of the amino acid sequence, alamethicin resembles a transmembrane domain in a typical transport/channel protein with several bilayer-spanning helices (Brandl and Deber, 1986).

The structure of alamethicin has been studied in the crystalline phase using x-ray diffraction (XRD) (Fox and Richards, 1982) and ^{13}C–^{13}C rotational resonance NMR (Peersen et al., 1992), in organic solutions using ^{1}H, ^{13}C, and ^{15}N nuclear magnetic resonance (NMR) (Banerjee et al., 1983; Esposito et al., 1987; Chandrasekhar et al., 1988; Yee and O'Neil, 1992; Kelsh et al., 1992; Yee et al., 1997), in amphiphilic (SDS micelles or POPC) environments using ^{1}H NMR (Franklin et al., 1994; Brachais et al., 1998; Jayasinghe et al., 1998), and investigated extensively using molecular dynamics (MD) simulations (Biggin et al., 1997; Gibbs et al., 1997; Breed et al., 1997; Sessions et al., 1998; Tieleman et al., 1999a–c). Independent of the peptide environment (crystals, organic solution, or micelles), these studies largely support the findings of Fox and Richards (1982), namely that alamethicin exists predominantly in an α-helical conformation over its entire length. This structure

Received for publication 19 September 2000 and in final form 31 May 2001.

Address reprint requests to Niels C. Nielsen, Laboratory for Biomolecular NMR Spectroscopy, Dept. of Molecular and Structural Biology, Science Park, Gustav Wieds Vej 10, University of Aarhus, DK-8000 Aarhus C, Denmark. Tel: +45-89423841; Fax: +45-86196199; E-mail: ncn@imsb.au.dk.

Dr. Hohwy's present address is Institut für Molekularbiologie und Biophysik, Eidgenössische Technische Hochschule, Hönggerberg, CH-8093 Zürich, Switzerland.

Dr. Thomsen's present address is Department of Protein Chemistry, Institute of Molecular Biology, University of Copenhagen, DK-1353 Copenhagen K, Denmark.

Dr. Adelhorst's present address is Dako A/S, Produktionsvej 42, DK-2600 Glostrup, Denmark.

0006-3495/01/09/1684/15 $2.00

conforms well with the high content of helix-stabilizing α-amino-isoburyric acid (Aib) residues. It is generally accepted that the structure contains a stable α-helical conformation in the N-terminal half of the sequence (residues 4–9 or 10), a less regular helix conformation in the C-terminal half (residues 12–16), and greater conformational flexibility for the residues outside these regions. The latter regions most likely include a more extended structure in the outer part of the C-terminal and potentially a bend near the Pro^{14} residue.

Despite a detailed picture of the overall structure of alamethicin, its conformation and orientation when associated with lipid bilayers and the mechanism by which it induces voltage-dependent ion conductance is still debated. Models involving a long-lived open pore of aggregated alamethicin helices in a transmembrane barrel-stave configuration (Baumann and Mueller, 1974) in the conductive state are accepted in most of the studies cited above. More discussion has concerned the conformation in the nonconductive state. Models ranging from monomeric and multimeric rods on the lipid surface (Baumann and Mueller, 1974; Banerjee et al., 1985; Biggin et al., 1997; Tieleman et al., 1999a; Kessel et al., 2000) via bent structures and preaggregates with the C-terminal segment anchoring on the lipid surface and the N-terminal segment extending into the membrane (Fox and Richards, 1982; Franklin et al., 1994) to purely transmembrane orientations (North et al. 1995; Barranger-Mathys and Cafiso, 1996; Breed et al., 1997; Jayasinghe et al., 1998; Tieleman, 1999b,c) have been proposed. The various models have been supported by circular dichroism (Wu et al., 1990; Huang and Wu, 1991; Wolley and Wallace, 1993), neutron in-plane scattering (He et al., 1996a,b), electron paramagnetic resonance (EPR) and NMR on spin-labeled alamethicin (Barranger-Mathys and Cafiso, 1994, 1996; Jayasinghe et al., 1998), and ^{2}H, ^{31}P (Banerjee et al., 1985), and ^{15}N solid-state NMR (North et al., 1995) experiments. These studies also demonstrated that the peptide-to-lipid concentration, the temperature, and the hydration are important parameters for the peptide–lipid and peptide–peptide interactions, and, thereby, for the configuration of alamethicin in the membrane. Furthermore, it has been investigated how the eight Aib residues, Pro^{14}, and the polar Gln^{7} residue are related to the structure, the channel formation, and function for alamethicin (Brachais et al., 1998; Sessions et al., 1998; Jaikaran et al., 1997; Dathe et al., 1998; Tieleman et al., 1999b).

Among the methods listed above, solid-state NMR of isotope-labeled peptides incorporated into macroscopically oriented phospholipid bilayers is particularly useful for obtaining detailed information about the structure, dynamics, and orientation of membrane-associated peptides and proteins at the atomic level (Bechinger et al., 1991, 1993; Ketchem et al., 1993; Ramamoorthy et al., 1995; Opella et al., 1999; Kovacs et al., 2000). Using this approach, North et al. (1995) demonstrated that the N-terminal part of alamethicin is oriented with the helix axis parallel to the bilayer normal. By arguments concerning motional averaging, this result was extended to suggest a straight transmembrane configuration of the entire peptide. Considering the large number of models suggesting a kink around the Pro^{14} residue and a flexible C-terminal of alamethicin potentially at the membrane surface in the nonconducting state, it is relevant also to consider the central and C-terminal parts of the peptide. Thus, in this study, the helix orientation(s) relative to the bilayer normal, including the potential for a proline-induced kink of the helix structure, are investigated in more detail using ^{15}N solid-state NMR on three alamethicin peptides differently labeled with ^{15}N at the Ala^{6}, Val^{9}, and Val^{15} residues. Furthermore, to investigate the role of the Aib residues a similar analysis is performed for an alamethicin analogue *Ac*-Ala-Pro-Aib-Ala-Aib-Ala-Gln-Aib-Val-Aib-Gly-Leu-Ala-Pro-Val-Ala-Aib-Glu-Gln-*Phol*, where three of the Aib residues (*underlined*) have been replaced by Ala. Finally, the structural constraints established using solid-state NMR for the various labeled alamethicins are analyzed in relation to the earlier XRD structure (Fox and Richards, 1982) and a series of model structures obtained in this work by modeling and molecular dynamics calculations. The results are discussed in light of previous models for alamethicin in monomeric forms as well as part of a multimeric ion channel.

MATERIALS AND METHODS

Sample preparation

Alamethicin ^{15}N-labeled on Ala^{6}, Val^{9}, and Val^{15} (three different peptides) was purchased from Quality Controlled Biochemicals, Inc. (Hopkinson, MA). The alamethicin analog with three of the Aib positions replaced by alanine (sequence given above) was prepared by solid-phase peptide synthesis (*t*-Boc chemistry) with ^{15}N-labeled amino acids at the Ala^{6} and Ala^{16} positions (two different peptides). The purity and quality of all peptides were tested by high pressure liquid chromatography and mass spectroscopy. ^{15}N-labeled t-BOC alanine was purchased from Cambridge Isotope Laboratories (Andover, MA). Dimyristoylphosphatidylcholine (DMPC) was obtained from Avanti Polar Lipids (Alabaster, AL). Both peptides and phospholipids were used without further purification.

The three differently ^{15}N-labeled alamethicin samples were prepared by co-dissolving 10 mg of the peptide (5.2 μmole) in 70 μl methanol (95%, spectroscopic grade) with 60 mg DMPC in 70 μl methanol corresponding to a peptide:lipid molar ratio of 1:8. For the alamethicin analogues we used the same proportionality but with a lower amount of peptide (5.5 mg). For each sample, the solution was distributed equally on 12 glass plates of dimension $10 \times 10 \times 0.1$ mm^3 cut from standard microscope coverslips (Menzel-Gläser, Germany) and rinsed carefully in methanol before use. The solvent was removed by first air drying overnight at ambient temperature and pressure and then evaporating 8 h under high vacuum. The samples were hydrated above de-ionized water in a closed dessicator (100% humidity) in 3 days at 23°C followed by 2 days at 43°C. The hydrated peptide/lipid mixtures were aligned into parallel multilayers by compressing the 12 glass plates in a stack. The stack was immediately placed in an airtight sample chamber made of Macor (Corning Glass Works, Corning, WY) equipped with a water reservoir to maintain the hydration constant throughout several days of NMR experiments with intense rf pulsing as described earlier (Nielsen et al., 1995).

Flat-coil NMR

^{15}N solid-state NMR experiments were performed at 30.40 and 40.52 MHz using Varian XL-300 (7.05 T) and Varian Unity-INOVA 400 (9.39 T) NMR spectrometers, respectively, equipped with home-built ^{15}N/^{1}H double-tuned flat-coil NMR probes (Nielsen et al., 1995). An rf field strength of 35 kHz was used for ^{1}H and ^{15}N during cross-polarization (CP) (Pines et al., 1973), whereas an rf field strength was 56 kHz for ^{1}H pulses and decoupling. All experiments used 2.5–3.5-s relaxation delay, 0.4–2.5-ms Hartman–Hahn contact period for CP, and a 20-ms acquisition period with ^{1}H decoupling. The rf coil (rectangular 4-turn flattened rf coil; inner dimension $8 \times 14 \times 4$ mm^3) and the sample chamber were oriented such that the bilayer normal was parallel to the static magnetic field (B_0). To avoid long-term deterioration (dehydration) of the sample induced by temperature gradients in the sample chamber during rf irradiation, the part of the chamber containing the sample was "cooled" by an air stream at 23°C, while the part with the water reservoir was "heated" by an air stream at 36°C (Nielsen et al., 1995). ^{15}N chemical shifts were determined using a standard CP experiment, whereas ^{1}H–^{15}N dipolar couplings were measured using a 2D separated local field (SLF) (Hester et al., 1975) experiment with BLEW-12 (Burum et al., 1981) homonuclear multiple-pulse decoupling in the t_1 period. We note that this experiment was chosen instead of the resolution-wise very attractive PISEMA experiment (Wu et al., 1994) because of the limited rf capabilities of our flat-coil NMR probe, which did not allow for well-resolved PISEMA spectra without folding ambiquities. All experiments were optimized using a single crystal of a doubly ^{15}N-labeled *N*-acetyl-L-valyl-L-leucine (*Ac*-Val-Leu) dipeptide. Prior to the ^{15}N experiments, the orientation of the DMPC bilayers in the hydrated peptide/lipid samples was checked using a standard ^{31}P single-pulse experiment at 7.05 T (121.4 MHz) providing information about the orientation of the ^{31}P chemical shift tensors for the phosphate headgroups in the phospholipids. The ^{15}N chemical shifts were referenced relative to an external saturated solution of $^{15}NH_4NO_3$ (we note that the isotropic chemical shift of $^{15}NH_4NO_3$ is -22.3 ppm relative to liquid $^{15}NH_3$).

Restriction plots

The orientation of a ^{15}N-labeled peptide plane relative to B_0, which coincides with the normal of the lipid bilayer, may be determined by measuring the orientation of the amide ^{15}N chemical shift and ^{1}H–^{15}N dipolar coupling tensors relative to B_0 and use empirical relations for the orientation of these tensors relative to the peptide plane (Opella et al., 1987; Bechinger et al., 1991; Wu et al., 1995). For this purpose, it is convenient to express the observed chemical shift (δ_{obs}, in ppm) and dipolar coupling (b_{obs}, in angular frequency) as

$$\delta_{obs} = \delta_{iso} + \delta_{aniso} \sum_{m'=-2}^{2} \sum_{m=-2}^{2} (R^{CS}_{2,m'})^{P} D^{(2)}_{m',m}(\Omega^{CS}_{PE}) d^{(2)}_{m,0}(\beta_{EL}) \exp\{-im\alpha_{EL}\}, \quad (1)$$

$$b_{obs} = b_{NH} \sum_{m=-2}^{2} D^{(2)}_{0,m}(\Omega^{NH}_{PE}) d^{(2)}_{m,0}(\beta_{EL}) \exp\{-im\alpha_{EL}\}, \quad (2)$$

where $\delta_{iso} = (\delta_{xx} + \delta_{yy} + \delta_{zz})/3$, $\delta_{aniso} = \delta_{zz} - \delta_{iso}$, $(R^{CS}_{2,0})^{P} = 1$, $(R^{CS}_{2,\pm1})^{P} = 0$, $(R^{CS}_{2,\pm2})^{P} = -\eta_{CS}/\sqrt{6}$, $\eta_{CS} = (\delta_{yy} - \delta_{xx})/\delta_{aniso}$, and $b_{NH} = -\gamma_I\gamma_S\hbar\mu_0/(4\pi r^3_{NH})$. δ_{ii} denotes the principal elements for the chemical shift tensor ($|\delta_{zz} - \delta_{iso}| \geq |\delta_{xx} - \delta_{iso}| \geq |\delta_{yy} - \delta_{iso}|$), $b_{NH}/2\pi$ the dipolar coupling constant, and r_{NH} the internuclear distance. *P* is the principal axis frame, *E* the peptide plane frame with x_E along N–H and z_E being the normal to the plane (Fig. 1 *A*), and *L* the laboratory-fixed frame. The coordinate systems are related by the Euler angles $\Omega_{PE} = \{\alpha_{PE}, \beta_{PE}, \gamma_{PE}\}$ and $\Omega_{EL} = \{\alpha_{EL}, \beta_{EL}, 0\}$ (Fig. 1 *B*). $D^{(2)}(\Omega)$ and $d^{(2)}(\beta)$ are second-rank Wigner and reduced Wigner matrices, respectively.

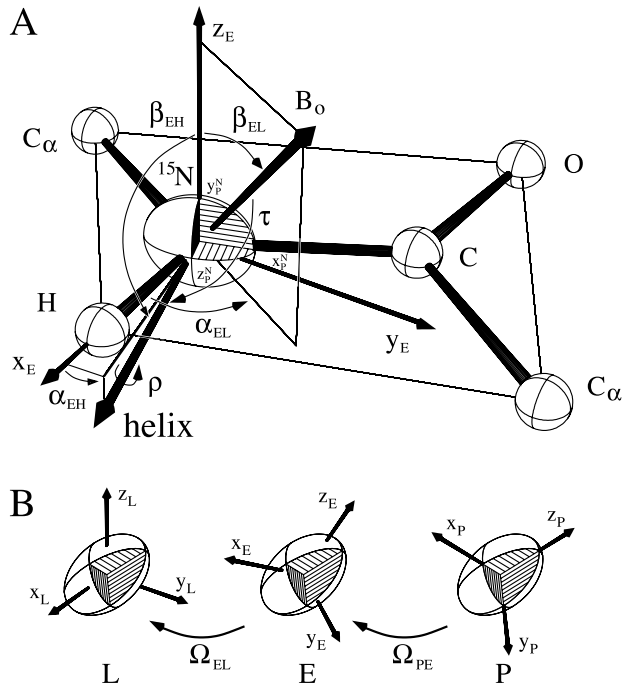

FIGURE 1 ORTEP-type representation. (*A*) The orientation of the ^{15}N chemical shift tensor, the ^{1}H–^{15}N dipolar coupling tensor (oriented along the N–H bond), and an ideal helix axis relative to the peptide plane (the principal elements and the Euler angles are given in the text) and the static magnetic field (B_0). (*B*) The Euler angles relating any of the principal axis frames (*P*) via the molecular frame (*E*) to the laboratory frame (*L*).

Using Eqs. 1–2 along with empirical values for the magnitudes (δ^N_{xx}, δ^N_{yy}, δ^N_{zz}, $b_{NH}/2\pi$) and orientations ($\Omega^{CS,N}_{PE}$, Ω^{NH}_{PE}) of the ^{15}N chemical shift and ^{1}H–^{15}N dipolar coupling tensors, the measured δ_{obs} and b_{obs} values may be interpreted in terms of the orientation of the peptide plane relative to the lipid bilayer. The possible solutions (considering uncertainties for the empirical and experimental parameters) are conveniently visualized by restriction plots showing the pairs of angles α_{EL} and β_{EL} compatible with the experimental values (Bechinger et al., 1991; Ramamoorthy et al., 1995). The magnitude and orientation of the ^{15}N chemical shift tensors relative to the peptide plane have been determined for several peptides (e.g., Harbison et al., 1984; Oas et al., 1987; Hartzell et al., 1987; Teng and Cross, 1989; Bechinger et al., 1991; Mai et al., 1993; Shoji et al., 1993; North et al., 1995; Ramamoorthy et al., 1995; Wu et al., 1995; Kovacs and Cross, 1997) and found to display relatively small variations. In this work, we assume that the ^{15}N chemical shift tensor is not subject to significant motional averaging beyond that induced by the fast motion about the bilayer normal as typically encountered in hydrated lipid samples. Thus, we assume the tensor characterized by the typical values of $\delta^N_{xx} = 30 \pm 5$ ppm, $\delta^N_{yy} = 53 \pm 5$ ppm, $\delta^N_{zz} = 195 \pm 5$ ppm, and $\Omega^{CS,N}_{PE} = \{-90°, -90°, -17 \pm 4°\}$, where the uncertainties accomodate residue and secondary structure-specific variations in the parameters. The tensor is oriented such that the δ_{yy} axis (y^N_P) is perpendicular to the peptide plane and the axis of the unique (least shielded) element δ_{zz} (z^N_P) being tilted $17 \pm 4°$ away from the N–H bond within the peptide plane as visualized by the ORTEP-type (Burnett and Johnson, 1996) plot in Fig. 1 *A*. We note that y^N_P in some studies (Wu et al., 1995) has been reported tilting away from the peptide plane normal by 10–30° (corresponding to $\alpha^{CS,N}_{PE} = -80°$ to $-60°$). This tilt only affects the restrictions marginally and has accordingly been disregarded in this study. The ^{1}H–^{15}N dipolar coupling tensor is axially

symmetric, aligned along the N–H internuclear axis (i.e., $\Omega_{PE}^{NH} = \{0°, -90°, 0°\}$), and characterized by the dipolar coupling constant $b_{NH}/2\pi = 9.9 \pm 0.2$ kHz (corresponding to an internuclear distance of $r_{NH} = 1.07$ Å) (Wu et al., 1995). For an ideal α-helix structure (specifically calculated using $\phi = \psi = -57°$) the orientation of the helix axis relative to the peptide-plane frame may, to a good approximation, be described by the Euler angles $\Omega_{EH} = \{13°, 91°, 0°\}$ as illustrated in Fig. 1 *A*. The angle between the helix axis and B_0 is denoted τ, and ρ denotes the rotational pitch around the helix axis. Based on these definitions, it is possible to establish restrictions between the helix tilt-angle τ and the pairs of angles α_{EL} and β_{EL} and thereby determine the tilt angle for a potential local α-helix axis relative to the normal of the bilayer.

All numerical simulations, generation of restriction plots, and iterative fitting to XRD, modeled, and molecular dynamics structures were accomplished on a 450-MHz Pentium-III workstation operating under Linux 6.1 using the SIMPSON solid-state NMR simulation package (Bak et al., 2000). Simulation and generation of restriction plots at 0.5° resolution for three peptide planes required 21 s of CPU time, whereas iterative fitting to model structures typically required a processing time of 1 min.

Molecular dynamics calculations and molecular modeling

MD calculations were performed in a simulated solvent designed to emulate the lipid bilayer environment (chloroform, dielectric constant 4.806 at 20 K, comparing reasonably with the dielectric constant of about 2–4 for the hydrocarbon region in lipid bilayers). The calculations were carried out on an SGI octane (IRIX64 6.5) workstation using the MMFF94S (planar sp2 N) force field implemented in the Macromodel (Mohamadi et al., 1990) modeling program. The simulations typically required 234 s of CPU time per nanosecond of simulation time. Each run had a starting temperature of 1000 K, running temperature of 300 K with a 0.2-ps coupling to a thermal bath, and a final temperature of 0 K. The total run time was 100 ps with a time step of 1.5 fs. Simple peptide backbone models involving various combinations of α-helix and 3_{10}-helix structure elements were generated using the WHAT IF program (Vriend, 1990) on a 450-MHz Pentium III workstation under Linux 6.1.

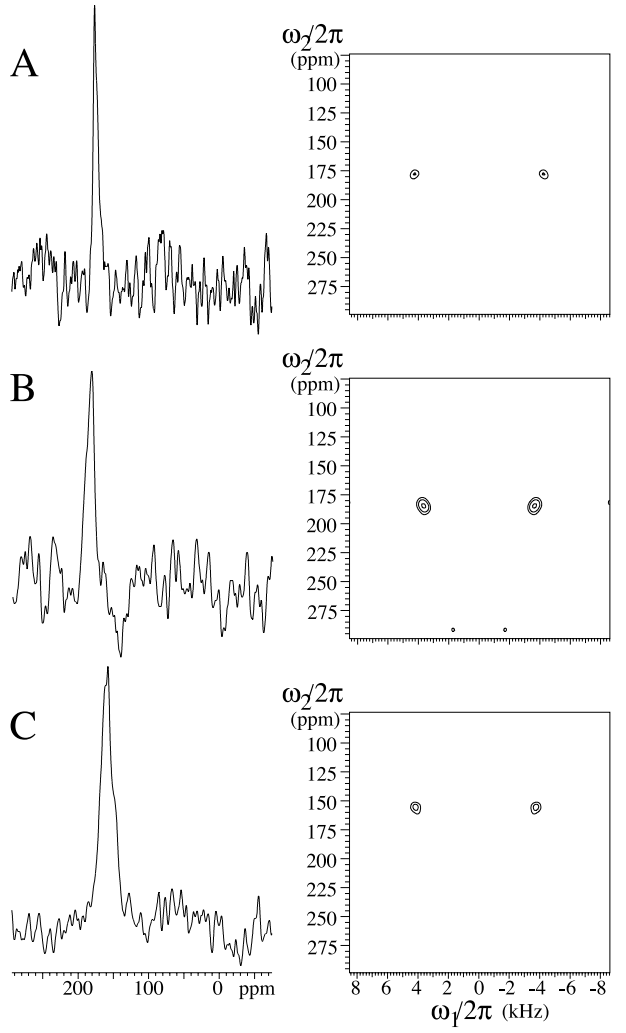

FIGURE 2 ^{15}N CP (*left column*) and ^{1}H–^{15}N 2D SLF (*right column*) spectra obtained at 9.39 T of (*A*) ^{15}N-Ala^{6}-, (*B*) ^{15}N-Val^{9}-, and (*C*) ^{15}N-Val^{15}-labeled alamethicin incorporated into hydrated DMPC bilayers (peptide:lipid ratio of 1:8) and oriented between glass plates arranged with the plane perpendicular to the B_0 direction. The spectra were recorded using 3.5-s relaxation delay, 2.5-ms Hartmann–Hahn contact time, 20,000–25,000 scans for the CP experiments, and 2700 scans for each of the 16 t_1 increments ($\Delta t_1 = 57.6$ μs) in the SLF experiments.

RESULTS

Solid-state NMR restrictions

Figure 2 shows ^{15}N CP and 2D ^{1}H–^{15}N SLF spectra for the three singly ^{15}N-Ala^{6}-, ^{15}N-Val^{9}-, and ^{15}N-Val^{15}-labeled alamethicin peptides incorporated with a peptide:lipid ratio of 1:8 into hydrated DMPC phospholipid bilayers and oriented with the membrane normal parallel to the magnetic field. We note that this peptide:lipid ratio is relatively high and in the regime where all molecules is expected to be inserted into the membrane as deduced by oriented circular dichroism (He et al., 1996b). Evidently, all NMR spectra contain a single narrow ^{15}N resonance in the $\delta_{obs} \approx 160$–180-ppm region with a line width at half height of 8–16 ppm. The actual values for the chemical shifts and dipolar couplings determined from the various experimental spectra are listed in Table 1. The relatively narrow ^{15}N resonances indicate that the peptides are, within a small margin, aligned uniformly with respect to the bilayer normal. This finding is supported by ^{31}P spectra (not shown), which, for the same samples, contain a single relatively narrow (line width 2–4 ppm) resonance at 28 ppm (relative to external 85% H_3PO_4) for the phosphate headgroups. This indicates a relatively small orientational distribution (i.e., mosaic spread) for the planar phospholipid bilayers. Furthermore, the ^{15}N chemical shifts are close to the low-field shoulder of the typical ^{15}N powder pattern for peptides in hydrated lipid membranes (in the present case corresponding to $\delta_{zz}^{N} = 195 \pm 5$ ppm). We note that the ^{15}N CP spectra (in particular for Ala^{6} and Val^{15}) give indication of a weak powder pattern with the most intense singularity around 50–55 ppm being compatible with the typical chemical shift values given above. From the measured chemical shifts, it can immediately be deduced that the amide ^{15}N chemical shift tensors

TABLE 1 ^{15}N Chemical shifts (δ_{obs}) and ^{1}H–^{15}N dipolar couplings ($b_{obs}/2\pi$) along with the associated restrictions (cf. Fig. 3) on α_{EL}, β_{EL}, and τ obtained by solid-state NMR for alamethicin ^{15}N-labeled at the Ala^6, Val^9, and Val^{15} residues and an alamethicin analog (see text) ^{15}N-labeled at the Ala^6 and Ala^{16} positions

Peptide	^{15}N label	δ_{obs}* (ppm)	$b_{obs}/2\pi^{\dagger}$ (kHz)	$\alpha_{EL}{}^{\ddagger,\S}$ (°)	$\beta_{EL}{}^{\S}$ (°)	$\tau^{\S,\P}$ (°)
Alamethicin	Ala^6	176 ± 5	8.9 ± 0.3	170–193	72–108	10–23
	Val^9	181 ± 5	7.8 ± 0.3	181–204	67–113	11–23
	Val^{15}	160 ± 5	8.4 ± 0.3	164–186	69–111	21–29
Alamethicin analog	Ala^6	174 ± 5	—	159–227	56–123	18–33
	Ala^{16}	154 ± 5	—	159–232	54–126	21–40

All peptides were incorporated into planar DMPC bilayers with a peptide:lipid ratio of 1:8.

*Relative to $^{15}NH_4NO_3$ (saturated aq. solution).

†Corrected for a scaling of 0.475 by BLEW-12 (Burum et al., 1981).

‡$\alpha_{EL} \pm 180°$ also applies.

§Calculated under the assumption of $\delta^N_{xx} = 30 \pm 5$ ppm, $\delta^N_{yy} = 53 \pm 5$ ppm, $\delta^N_{zz} = 195 \pm 5$ ppm, $\Omega^{CS,N}_{PE} = \{-90°, -90°, -17 \pm 4°\}$, $b_{NH}/2\pi = 9.9 \pm 0.2$ kHz, and $\Omega^{NH}_{PE} = \{0°, -90°, 0°\}$.

¶Obtained from the intersection between the experimental α_{EL}, β_{EL} restrictions and the theoretical restrictions representing local α-helix structures ($\phi = \psi = -57°$) oriented relative to the peptide plane as $\Omega_{EH} = \{13°, 91°, 0°\}$ and with the helix axis inclined by the angle τ to the bilayer normal.

for Ala^6, Val^9, and Val^{15} all have z^N_P (corresponding to δ^N_{zz}) and thereby the N–H internuclear axis (cf. Fig. 1 *A*) aligned approximately parallel to B_0, i.e., $\beta_{EL} \approx 90°$. Assuming that alamethicin (as in methanol and micelle environments) largely adopts an α-helical secondary structure where the helix axis within 10–15° (see below) is parallel to the N–H axis, this information suggests that the peptide over its entire length is configured in a transmembrane orientation relative to the planar DMPC bilayers. This first conclusion is supported by the ^{1}H–^{15}N dipolar splittings ($b_{obs}/2\pi$), which impose complementary restrictions to the orientation of the peptide planes relative to B_0, because the N–H dipolar coupling tensor is oriented differently than the ^{15}N chemical shift tensor relative to the peptide plane (see Fig. 1 *A*). By direct comparison of the orientation-dependent dipolar couplings ($b_{obs}/2\pi$) of 8.9, 7.8, and 8.4 kHz (compensated for scaling by BLEW-12 irradiation) measured for the Ala^6, Val^9, and Val^{15} ^{15}N-labeled alamethicins, respectively, with the nonscaled dipolar coupling of $b_{NH}/2\pi = 9.9$ kHz, the angle between the N–H bond vector and the B_0 direction may be estimated to be in the order of 14–18°.

To exploit more rigorously the structural constraints from the δ_{obs} and $b_{obs}/2\pi$ values and thereby obtain a more detailed picture of the conformation of alamethicin in phospholipid bilayers, it is useful to use these values along with the empirically established tensor versus peptide plane information (cf. Fig. 1 *A*) to generate restriction plots for the allowed α_{EL} and β_{EL} Euler angles. Restriction plots corresponding to δ_{obs} and $b_{obs}/2\pi$ individually and in combination (the intersection of the two plots) determined for the Ala^6, Val^9, and Val^{15} peptide planes in the three differently ^{15}N-labeled alamethicin samples are shown in Fig. 3. In these plots, the black areas represent pairs of α_{EL} and β_{EL} angles that are compatible with the experimental data within the limits of the estimated uncertainties on the experimental and empirically established tensor parameters. From the intersection plots it is seen that all three peptide planes are compatible with β_{EL} values in the vicinity of 90° with an α_{EL}-dependent variation of ±18°, ±23°, and ±21° for Ala^6, Val^9, and Val^{15}, respectively. α_{EL} displays variations in the angular regions 170–193° (Ala^6), 181–204° (Val^9), and 164–186° (Val^{15}) depending on β_{EL}.

Within the assumption that the peptide planes individually are parts of ideal (and possibly only local) α-helical structures, the allowed pairs of α_{EL} and β_{EL} angles may be rationalized by comparison with restrictions corresponding to different helix tilt angles τ calculated using $\Omega_{EH} = \{13°, 91°, 0°\}$ and included as grey contours in the intersection plots of Fig. 3. This representation reveals that the experimental α_{EL}, β_{EL} restrictions are compatible with tilted α-helices characterized by τ angles in the order of 10–23°, 11–23°, and 21–29° for the Ala^6, Val^9, and Val^{15} peptide planes, respectively. As an interesting result, it appears that none of the restrictions are compatible with a pure α-helix crossing the membrane with the helix axis parallel to the bilayer normal (i.e., $\tau = 0°$). It is also evident that the two labeled N-terminal residues are compatible with slightly smaller helix tilt angles than the labeled C-terminal residue. We note that this observation is even more pronounced if we compare the experimental restrictions with those from a regular 3_{10} helix (calculated using $\Omega_{EH} = \{25°, 100°, 0°\}$ corresponding to a helix with $\phi = -50°$ and $\psi = -20°$ for all residues), which, for comparison, is included in the dipolar coupling restriction plot for the Val^{15} residue in Fig. 3 *C*. This plot indicates compatibility between the experimental restrictions for Val^{15} with a local 3_{10} helix tilting by as much as $\tau = 25–45°$ relative to the bilayer normal. Finally, it is interesting to note that the restrictions for the three residues taken individually (i.e., not coupled in a structure, see below) all would intuitively be compatible with a straight α-helix tilting 21–23° relative to the bilayer normal. The impact of the average angles of 16° (Ala^6), 17° (Val^9), and 25° (Val^{15}) on the orientation of the individual peptide planes relative to the bilayer normal is visualized

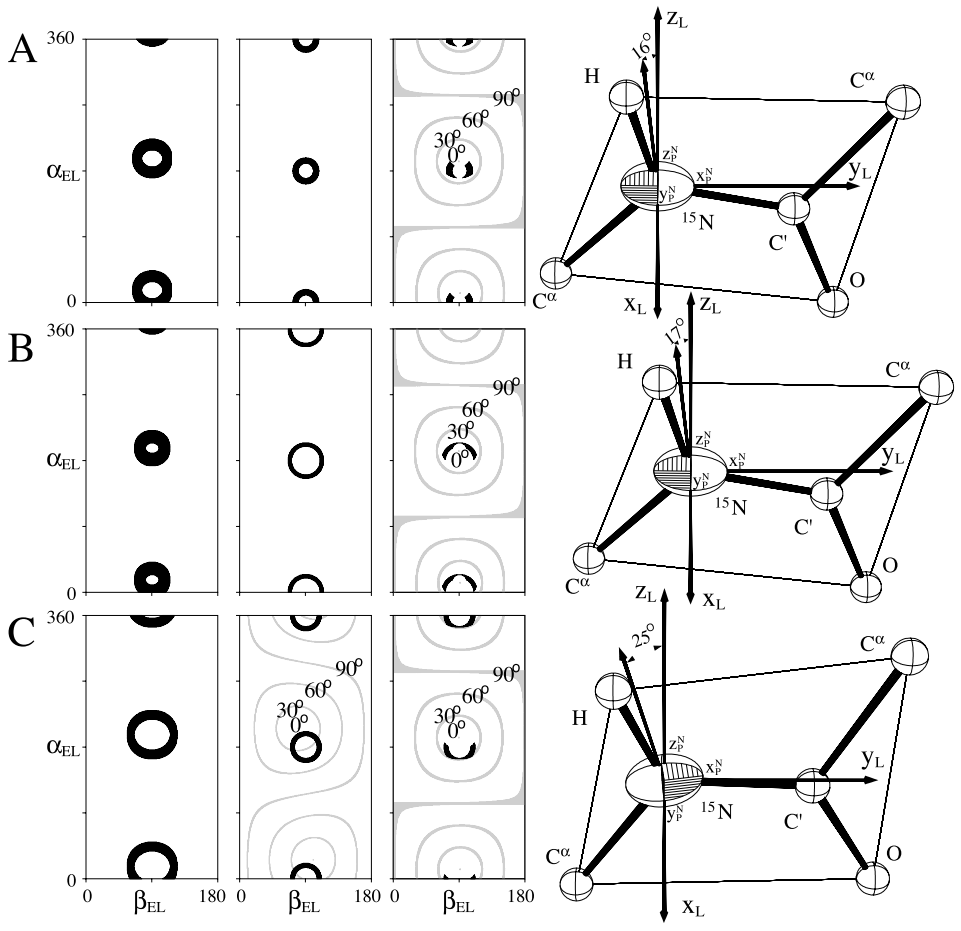

FIGURE 3 Restriction plots (*left three columns*) and orientation of peptide planes and helix axes relative to the laboratory frame (*right column*, $z_L \| B_0$) for (*A*) ^{15}N-Ala^6, (*B*) ^{15}N-Val^9, and (*C*) ^{15}N-Val^{15} alamethicin corresponding to the parameters in Table 1. The restriction plots for the chemical shift (*first column*), dipolar coupling (*second column*), and their intersection (*third column*) takes into account uncertainties of ± 5 ppm and ± 0.3 kHz for the experimental δ_{obs} and $b_{obs}/2\pi$ values, respectively, as shown in Table 1 and visualized by ORTEP-type plots in the fourth column of this figure. The intersection plots include shaded restrictions corresponding to ideal local α helices with different tilt angles τ relative to the bilayer normal. For comparison, the dipolar coupling restriction plot in (*C*) also includes similar contours for an ideal 3_{10} helix (see text).

graphically in the right-hand side of Fig. 3. All orientational restrictions for the different peptide planes are summarized in Table 1.

To examine the influence of the helix-stabilizing Aib residues on the conformation of alamethicin in phospholipid bilayers, we measured the ^{15}N chemical shifts for a similarly prepared sample of an analog of alamethicin *Ac*-Ala-Pro-Aib-Ala-Aib-Ala-Gln-Aib-Val-Aib-Gly-Leu-Ala-Pro-Val-Ala-Aib-Glu-Gln-*Phol* differing from alamethicin in the exchange of the Aib residues 1, 13, and 16 by alanine. Figure 4 shows ^{15}N CP spectra for two different versions of this peptide ^{15}N-labeled at the Ala^6 and Ala^{16} positions and incorporated into an oriented DMPC bilayer using the procedure described above. In full consistency with the spectra for alamethicin, these samples yield a single ^{15}N resonance (20–30-ppm line width) in the low-field region of the typical ^{15}N amide powder spectrum. The specific δ_{obs} values of 174 and 154 ppm determined for the Ala^6 and Ala^{16} samples, respectively, lead to the $\{\alpha_{EL}, \beta_{EL}\}$ and τ restrictions represented graphically in the right-hand side of Fig. 4. Clearly, the ^{15}N chemical shifts and, accordingly, the solid-state NMR orientational restrictions are very similar to those observed for the original peptide and thereby compatible to a peptide with local α-helical secondary structures tilting by 5–25° and 15–35° relative to the bilayer normal in vicinity of the Ala^6 and Ala^{16} residues, respectively. Comparing the results obtained for alamethicin and its analog, it is interesting to note that, consistently, the chemical shifts observed in the C-terminal end are slightly smaller than those observed for the central and N-terminal part of the peptide. This may potentially be ascribed to a less regular helical structure in this part of the peptide. Finally, it should be noted that the similarity between the conformation of alamethicin and its Aib-deficient analog agrees well with the findings of Cafiso and coworkers (Barranger-Mathys and Cafiso, 1996; Jayasinghe et al., 1998) using EPR on various spin-labeled derivatives of alamethicin.

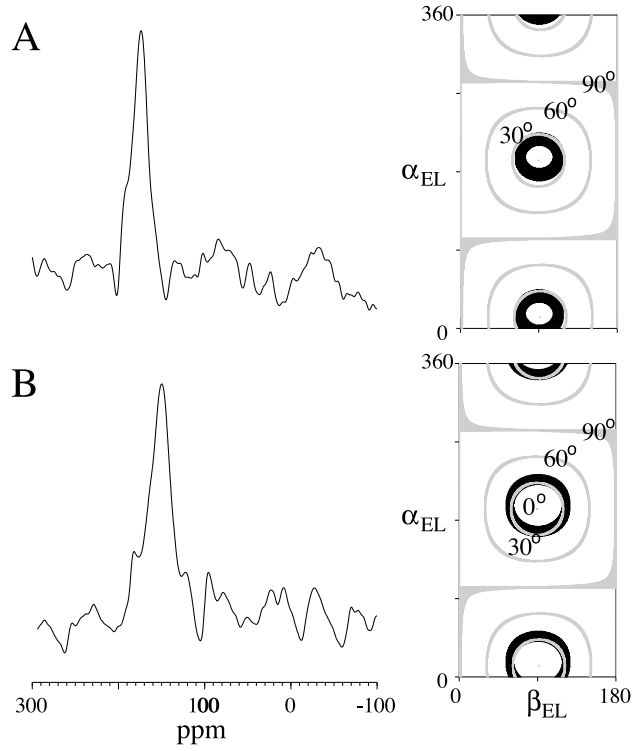

FIGURE 4 ^{15}N CP NMR spectra (*left column*) and restriction plots (*right column*) determined for the alamethicin analog *Ac*-Ala-Pro-Aib-Ala-Aib-Ala-Gln-Aib-Val-Aib-Gly-Leu-Ala-Pro-Val-Ala-Aib-Glu-Gln-*Phol* with ^{15}N-labeling at the (*A*) Ala^{6} and (*B*) Ala^{16} residue. The experimental spectra were recorded at 7.05 T using CP with 1000-μs contact time, 3-s relaxation delay, and (*A*) 130,000 and (*B*) 110,000 scans.

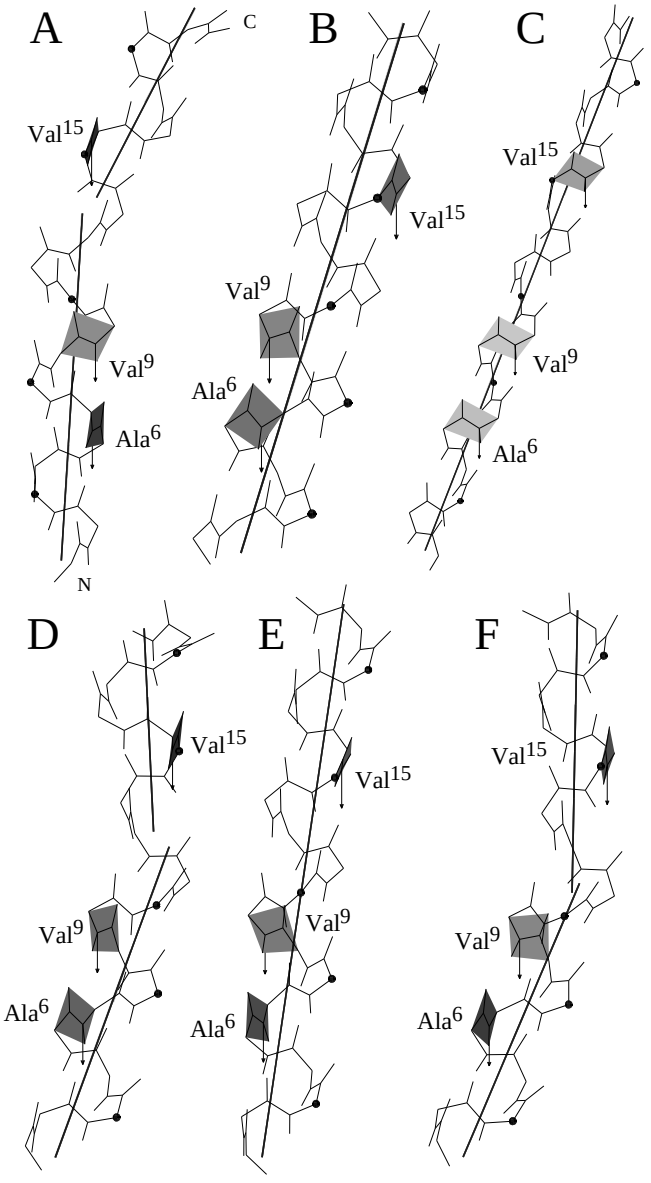

FIGURE 5 Representative backbone structures for various alamethicin models. (*A*) The XRD-structure determined by Fox and Richards (1982). (*B*) An ideal α-helix ($\phi = \psi = -57°$). (*C*) An ideal 3_{10} helix ($\phi = -50°$, $\psi = -20°$). (*D*) A 100-ps wild-type MD structure. (*E*) A 100-ps Pro^{14} to Ala^{14} mutant MD structure. (*F*) A 100-ps MD structure initialized with forced 3_{10} structure for the C-terminal (see text). For all structures, the orientation of the peptide (specified by the τ and ρ angles in Table 2) have been optimized for optimum agreement with the α_{EL} and β_{EL} structure contraints determined by solid-state NMR. The vertical axis and the black arrows at the ^{15}N position of each labeled peptide plane represents the orientation of the B_0 field. The plane of the paper corresponds to $\rho = 0$. The black dots represents C_α carbons of the hydrophilic Aib^{3}, Gln^{7}, Aib^{10}, Pro^{14}, and Glu^{18} residues.

Structure models

With the experimental data interpreted in terms of the orientation of the individual peptide planes relative to the membrane normal, it is relevant to examine in more detail potential consequences of the combination of these local structure constraints on the overall structure of alamethicin in phospholipid bilayers. For this purpose, we analyze the compatibility of the solid-state NMR data with the XRD structure of crystalline alamethicin, a series of simple backbone structures involving different combinations of α- and 3_{10}-helix secondary structure elements, and structures obtained by molecular dynamics calculations. The backbone structures for a representative set of the proposed models are visualized in a 3D Geomview representation (Levy et al., 1996) in Fig. 5 with specification of the three labeled peptide planes and average molecular axes for the N- and C-terminal ends of the molecule (see below). Figure 6 gives a graphical representation of the ϕ and ψ backbone torsion angles for the same set of structures.

The coordinates for the XRD structure (Fox and Richards, 1982) in Fig. 5 *A* were obtained from the Protein Data Bank (http://www.rcsb.org/pdb/; PDB ID: 1amt). A series of ideal 20-residue peptide backbone structures were generated to model fully α-helical ($\phi = \psi = -57°$, Fig. 5 *B*), fully 3_{10}-helical ($\phi = -50°$, $\psi = -20°$, Fig. 5 *C*), and various mixtures of such α- and 3_{10}-helices with the n N-terminal residues being α-helical and the $20 - n$ C-terminal residues being composed of 3_{10}-helix elements

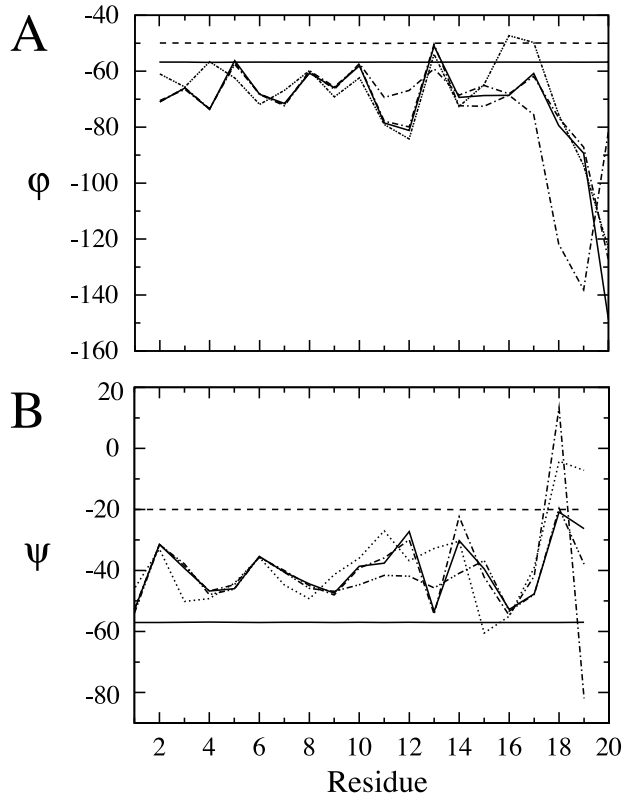

FIGURE 6 (*A*) ϕ and (*B*) ψ torsion angles for the six structures shown in Fig. 5, including the XRD structure (*dotted line*), an ideal α-helix (*solid line*), an ideal 3_{10} helix (*dashed line*), and wild-type (*dot-dashed line*), Pro^{14} to Ala^{14} mutant (*dot-dot-dashed line*), and 3_{10}-forced (*dot-dot-dot-dashed line*) MD calculations.

using *n* values of 12–14. The latter crude models have been inspired by the structures determined by XRD, solution NMR, and molecular dynamics calculations, which all, in some respect, support models with extended structures in the C-terminal of alamethicin. Finally, to investigate the propensity of alamethicin to change its conformation, a series of molecular dynamics calculations were performed using chloroform as a model solvent, which, with respect to dielectric constant, closely resembles the present lipid bilayer environment. Three series of calculations were conducted including wild type alamethicin, a mutant with Pro^{14} exchanged with Ala, and alamethicin with the C-terminal portion initially forced into a 3_{10} geometry. All variants largely retain (or re-acquire, in the case of the 3_{10} geometry) an α-helical structure after 100 ps as judged using the DSSP program (Kabsch and Sander, 1983) although the ϕ and ψ profiles for the various structures display some variation (Fig. 6), especially in the regions around the C-terminal phenylalaninol and the central Gly^{11}-X-X-Pro^{14} motif. We note that the ϕ and ψ angles over the first 16–17 residues for all structures are quite close to the average values of $\phi = -62°$ and $\psi = -41°$ determined in a survey over helices in a large number of protein crystal structures (Barlow and Thornton, 1988).

For the wild-type MD calculation, the structure (Fig. 5 *D*) remains essentially unchanged after 100 ps, except that the C-terminal phenylalaninol residue becomes slightly unwound relative to the starting structures (all the structures showed similar behavior in this respect). It has been shown in both model peptide studies (von Heijne, 1991; Ballesteros and Weinstein, 1992; Deber et al., 1990; Piela et al., 1987; Nilsson et al., 1998; Jacob et al., 1999) and from crystal structures of membrane proteins (Bywater et al., 2001) that proline residues sometimes have a tendency to cause a distortion in the helix. This is due to the lack of a hydrogen bond between the imido N atom of the proline and the carbonyl oxygen of the $(i - 3)$th preceding residue. This is commonly referred to as a "kink." Although this is by no means universal, when such a kink occurs, one observes that the ϕ angles of the $(i - 3)$th residue is in the range $-115°$ to $-135°$ and that of the $(i - 4)$th residue is $\sim -100°$ (Bywater et al., 2001). Often there is an out-of-plane distortion of the $(i - 1)$th peptide bond by up to $\sim -20°$. In the wild-type peptide, the value of the ϕ angle of the $(i - 3)$th residue (Gly^{11}) does depart somewhat from the standard α-helix values, but the $(i - 2)$th residue (Leu^{12}) is, if anything, more distorted, with not only slightly deviant ϕ and ψ angles but a distinctly nonplanar peptide bond ($\sim 10°$ out of plane). The distance between the Pro^{14} imido N and the carbonyl O of the $(i - 3)$th residue is 4.4 Å. This would normally be 2.8 Å if a hydrogen bond had been possible at this site. Nevertheless, the DSSP program regards the entire peptide as being α-helical.

For the Pro^{14} to Ala^{14} mutant (Fig. 5 *E*), no major changes were observed during the simulations. The slight kinking referred to for the wild type appears here too, but much less pronounced. This time the $(i - 1)$th peptide bond is almost planar but the $(i - 2)$th peptide bond is about 7° out of plane. The hydrogen bond distance between the Ala^{14} amide N and Leu^{11} carbonyl O is 3.3 Å, which is at the outer limit of what can be classified as a hydrogen bond. Likewise, the 3_{10}-forced structure (Fig. 5 *F*) reverts to an α-helix, with the exceptions that the Pro^{14} and Leu^{12} residues develop somewhat deviant ϕ, ψ, and ω torsion angles. To judge from the starting structure, this is more a memory from the structure prior to the enforced change in geometry to the 3_{10}-helix conformation in the C-terminal region, rather than a memory from the forced conformation. This suggests that the departures from true α-helix geometry do derive from the presence of a proline. It should be reiterated that these deviations in the torsion angles are not sufficient for a secondary structure-determination program like DSSP to consider that the helix is kinked, and to the extent that they are departures from classical α-helix geometry, they are very different from those commonly claimed (e.g., Bywater et al., 2001) as being the kink introduced by proline. Overall, these observations agree favorably with the conclusions of previous MD simulations in solution and in lipid bilayers (Breed et al., 1997; Tieleman et al., 1999b,c).

TABLE 2 Compatibility between the solid-state NMR restrictions and various backbone model structures for alamethicin

Structure	RMSD*	τ[†] (°)	ρ[‡] (°)	τ_N[§] (°)	τ_C[§] (°)	Backbone[¶] length/height (Å)	Hydrophic[‖] length/height (Å)
XRD**	13.6	12	26	5	28	30.0/28.5	22.0/21.7
α-helix[††]	4.2	17	341	–	–	24.7/23.4	18.5/17.1
3_{10}-helix[††]	5.7	21	244	–	–	38.6/36.1	28.3/26.1
1-12: α-helix, 13-20: 3_{10}-helix[††]	12.1	12	250	15	17	30.3/29.5	20.3/19.5
1-13: α-helix, 14-20: 3_{10}-helix[††]	30.0	12	255	19	3	29.7/29.3	20.0/19.1
1-14: α-helix, 15-20: 3_{10}-helix[††]	16.4	8	188	12	12	29.1/29.0	19.7/19.4
Wild-type MD	5.1	11	232	20	3	26.5/25.8	20.8/20.2
Pro^{14} to Ala^{14} mutant MD	9.5	8	234	–	–	28.8/28.6	21.2/20.8
3_{10}-forced MD	6.4	13	219	24	9	27.3/26.9	20.7/19.5

*RMSD = $\Sigma \sqrt{(\Delta\alpha_{EL})^2 + (\Delta\beta_{EL})^2}$, where $\Delta\alpha_{EL}$ and $\Delta\beta_{EL}$ denote the deviations between the α_{EL} and β_{EL} angles for the model structure and the closest set of the corresponding angles in the experimental restrictions. The summation runs over the three labeled peptide planes.

[†]Tilt angle between the average molecular axis and the membrane normal (i.e., B_0).

[‡]Rotation around the molecular axis (positive, counterclockwise looking toward the C-terminal), starting from the position where the direction from the helix axis to C_α for the first residue follows the positive tilt direction around the center of the molecule.

[§]Tilt angles for the average molecular axis through the N- (τ_N) and C- (τ_C) terminal residues with the breakpoint at residue 11 (3_{10}-forced MD), 12 (wild-type MD), 13 (XRD), and τ_N and τ_C reflect the two structure elements for the α- and 3_{10}-helix combinations. These angles are not given for largely straight structures.

[¶]Distance/height (projection) between the C^α in Aib^1 to $Phol^{20}$ (2–3 Å shorter than the full peptide including side chains).

[‖]Estimated to the distance/height (projection) from N in Pro^2 to N in Aib^{16}.

**Structure determined by Fox and Richards (1982).

[††]Simple models calculated using torsion angles of $\phi = \psi = -57°$ (α-helix) and $\phi = -50°$, $\psi = -20°$ (3_{10}-helix).

Compatibility between solid-state NMR restrictions and structure models

The compatibility between the various backbone structures and the orientational constraints for the three ^{15}N-labeled peptide planes obtained by solid-state NMR may be evaluated numerically by varying the overall orientation of the peptide relative to the B_0 direction (i.e., the bilayer normal). Different orientations will lead to different chemical shift and dipolar coupling parameters and thereby orientational restrictions on the α_{EL} and β_{EL} angles, which may be compared to the experimentally established restrictions. The overall orientation of the peptide may be described by a tilt angle τ of the average helix axis with respect to the membrane normal and a rotational pitch angle ρ around the helix axis (Fig. 1 *A*). Using this notation, the root-mean-square deviation (RMSD) between the actual τ- and ρ-dependent α_{EL} and β_{EL} angles and the closest pair of angles within the experimental restrictions (summed over the three peptide planes) may be minimized using Levenberg–Marquardt nonlinear regression (Bard, 1974) to define the optimum orientation of the peptide relative to the bilayer normal. Because the RMSD function typically is only partially continuous in this case (in particular for large τ values) and may have several local minima, this procedure was supplemented by a grid search over the two variables to ensure determination of a global minimum on the RMSD surface. We note that the rotational pitch, in general, may vary over the full 0–360° range, with its reference point fixed to a well-defined molecular axis (defined in Table 2), while the tilt angle typically will be searched in the area of 0–45°, corresponding to the tilt angles reported for transmembrane helices so far (e.g., Bowie, 1997; Kukol et al., 1999; Marassi et al., 1999).

Typical RMSD curves are shown in Fig. 7, which, for the purpose of further discussion, reflect optimization of the orientations for the XRD structure, the straight α-helix, and the 100-ps wild-type MD structures represented in Fig. 5, *A*, *B*, and *D*, respectively. Clearly, in all three cases, the optimization leads to a well-defined minimum at $\tau = 12°$ and $\rho = 26°$ for the XRD structure, $\tau = 17°$ and $\rho = 341°$ for the ideal α-helix, and $\tau = 11°$, and $\rho = 232°$ for the wild-type MD structure. Furthermore, from the minimum RMSD values, it appears that the two theoretical model structures (RMSD = 4.2–5.1) are in somewhat better agreement with the solid-state NMR restrictions than is the XRD structure (RMSD = 13.6). It should also be noticed that the solid-state NMR restrictions appear not to support peptides crossing the membrane with the molecular axis parallel to the bilayer normal. For example, the RMSD value for the ideal α-helix with $\tau = 0°$ is 22, being a direct measure for the considerable angular distance between the experimental restrictions and central grey helix-tilt contour (*dot*) in the restriction plot in the third column of Fig. 3. With the structures tilted away from the B_0 direction, we also observe a characteristic dependency on the rotational pitch angle ρ, which will be addressed later with specific attention to the XRD and wild-type MD structures. The optimum tilted conformations for various models are visualized graphically in Fig. 5, where the bilayer normal is vertical as indicated by the black arrows located at each of the labeled peptide

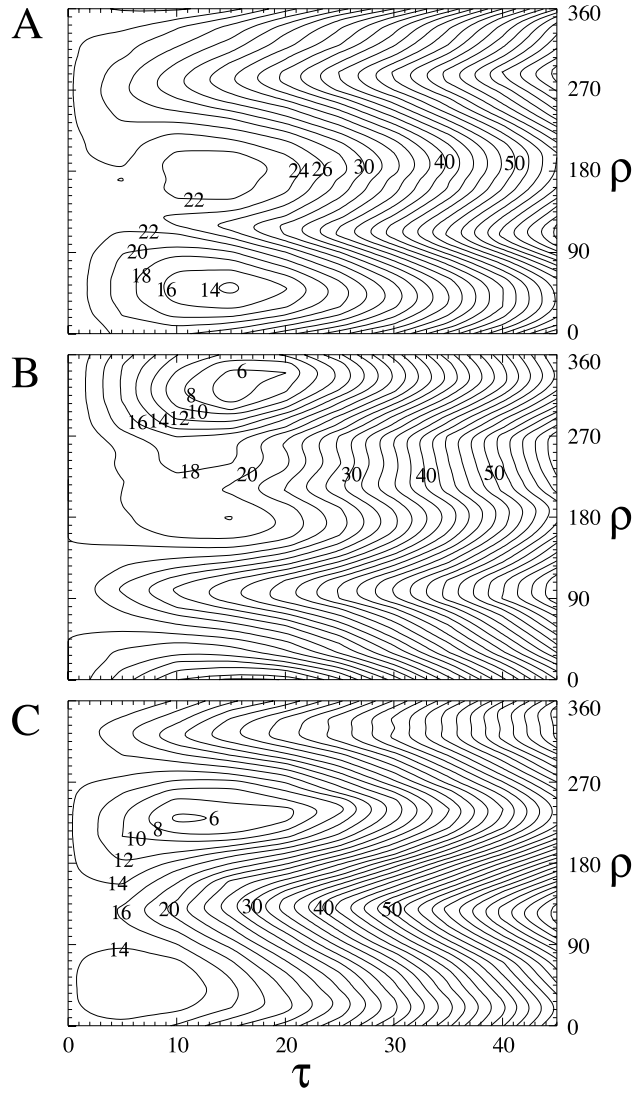

FIGURE 7 RMSD between the alamethicin solid-state NMR restrictions and structural constraints from (*A*) the XRD structure (Fox and Richards, 1982), (*B*) a straight α-helix ($\phi = \psi = -57°$), and (*C*) the 100-ps wild-type MD structure as function of the tilt-angle τ between the molecular axis and the bilayer normal and the rotational pitch ρ around the molecular axis. The optimimum orientations corresponding to the different structures are visualized in Fig. 5.

planes. As exemplified by the wild-type MD structure (Fig. 5 *D*), some of the models display a minor kink within the Gly^{11}-X-X-Pro^{14} motif, which conveniently may be characterized by specification of tilt angles τ_N and τ_C for the average molecular axes of the N- and C-terminals of the peptide, respectively, relative to the bilayer normal. Thus, for this specific structure, the $\tau = 11°$ tilt angle represents an average picture of N- (residues 1 to 12) and C-terminal (residues 13 to 20) structure elements tilting with as different angles as $\tau_N = 20°$ and $\tau_C = 3°$ relative to the bilayer normal. We note that the overall kink of $\sim 17°$ for this structure is in good agreement with model structures earlier reported, e.g., by Sansom and coworkers (Breed et al., 1997; Tieleman et al., 1999b).

Optimized orientation parameters for the various model structures, including those obtained by XRD (Fox and Richards, 1982) and molecular dynamics calculations, are summarized in Table 2 with the optimum membrane configuration for several of the models illustrated in Fig. 5. In addition to the various tilt angles, Table 2 also includes numbers for the overall length of the peptide backbone and the hydrophobic core region of the peptide as well as the height (projection) of these along the bilayer normal when adopting the optimum tilted conformation. Overall, this analysis indicates that the optimum configuration for all models require a tilt of the molecular axis by angles of 8–21° relative to the bilayer normal. Furthermore, among the nine investigated structures, it appears that the solid-state NMR data are most compatible with the straight α-helix (RMSD = 4.2), the wild-type 100-ps MD structure (RMSD = 5.1), and the straight 3_{10} helix (RMSD = 5.7), which all are associated with a somewhat lower RMSD value than the XRD structure (RMSD = 13.6). In the evaluation of these numbers, however, it is important to keep in mind that we, for practical reasons, consider only a limited number of model structures, and the compatibility check of these takes their origin in structural constraints from only 3 out of 20 amino acids. This provides, on one hand, an interesting test on the utility of very few constraints in structural analysis but, on the other hand, also implies that it is important to critically evaluate the solutions in relation to earlier findings and general rules concerning the relation between primary and secondary structures for amino acid sequences.

DISCUSSION

Although the tilted 3_{10} structure in Fig. 5 *C* matches the experimental restrictions quite well, it is probably not the most realistic solution for several other reasons. First, this structure is incompatible with all experimental and molecular simulation data established so far in the sense that none of these suggest an extended helix in the N-terminal of the peptide. Second, the hydrophilic Aib^3, Gln^7, Aib^{10}, Pro^{14}, and Glu^{18} residues (C_α carbons marked by black dots in Fig. 5 *C*) are not prevailingly located on one side of the peptide as would be expected for an amphipatic ion-channel peptide. Third, even with a tilt angle $\tau = 20°$, this peptide would have an overall backbone height (i.e., projection onto the bilayer normal) of 36 Å along bilayer normal, which is significantly larger than the hydrophobic (hydrocarbon) region of the phospholipid bilayer and may thereby force some of the hydrophobic residues into the polar outer regions of the bilayer. That this indeed may be the case becomes evident by comparing the thickness of 23–24 Å for the hydrophobic region of a fully hydrated DMPC bilayer (Lewis and Engelman, 1983; Scherer, 1989) with an esti-

mated height of 26 Å for the hydrophobic region of the peptide along the bilayer normal. Thus, although the Aib^{16} and Aib^{17} very well could be part of the polar C-terminal anchor outside the lipid hydrocarbon region (Barranger-Mathys et al., 1994, 1996; Kessel et al., 2000) this unfavorable match would either expose one of the hydrophobic Val^{15} or Pro^{2} residues to the polar water–phosphate surface of the membrane or require considerable deformation of the bilayer. In this context, it is relevant to note that recent studies have described a decrease in the bilayer thickness as an element in hydrophobic matching between ionophores and phospholipid bilayers (Harroun et al., 2000; Kessel et al., 2000).

For several reasons, the low-RMSD straight α-helix (Fig. 5 *B*) and wild-type MD (Fig. 5 *D*) structures represent more realistic models than does the 3_{10} helix for alamethicin in DM PC phospholipid bilayers. First, they are largely compatible with all available secondary structure information. Second, due to more compact structures (17–20-Å height of the hydrophobic region), they offer better conditions for hydrophobic match to the hydrated DMPC bilayers. Third, both structures have the hydrophilic Aib^{3}, Gln^{7}, Aib^{10}, Pro^{14}, and Glu^{18} residues and their polar side chains located on the same side of the peptide, regarded as important for the amphipatic character of the peptide and for the polar lining in the aqueous lumen of a multimeric alamethicin pore. Furthermore, in accord with earlier findings (Breed et al., 1997), the aromatic side chains and the hydroxyl group of the C-terminal $Phol^{20}$ are located at the opposite side of the peptide (i.e., the exterior of a potential helix bundle) being compatible with models where the C-terminal forms an anchor to the phosphate groups in the lipid–water surface. Among the two structures, the tilted α-helix benefits from the lowest RMSD value and could represent a reasonable model for alamethicin inserted into lipid bilayers, which may have a helix-stabilizing or straightening-out effect on the proline-induced kink (Schwarz et al., 1986; North et al., 1995). In particular, the adoption of a more regular α-helical structure in the C-terminal than the more extended structures deduced by solution NMR (Franklin et al., 1994) and XRD (Fox and Richards, 1982) would be possible considering that the conformation of the partly flexible C-terminal may undergo substantial conformation changes upon transfer from water/methanol or crystal to phospholipid bilayer environments. That this indeed may be the case has recently been investigated by Kessel et al. (2000) using continuum solvent model calculations of alamethicin–membrane interactions and by Tieleman et al. (1999b,c) using molecular dynamics calculations in solution and membrane environments. Likewise, the tilt of the helix by 17° relative to the bilayer normal may be reasonable, seen in the light that numerous structural studies of membrane proteins recently have reported tilt angles in this order for transmembrane α-helices in membrane proteins (e.g., Bowie, 1997).

The 100-ps wild-type MD structure (Fig. 5 *D*), with the average molecular axis tilted by 11° relative to be bilayer normal, also gives quite a good match to the solid-state NMR restrictions and contains all currently debated elements in its structure. This includes a reasonably sized kink within the Gly^{11}-X-X-Pro^{14} motif, a partly unwound structure in the C-terminal, and good conditions for polar lining inside a multimeric pore. For this model, it is interesting to note that the overall tilt of the molecule is induced by a substantial tilt of the N-terminal ($\tau_N = 20°$) as opposed to a largely transmembrane-oriented C-terminal ($\tau_C = 3°$). This optimum orientation of the peptide relative to the membrane differs from the common picture inspired from the early XRD work of Fox and Richards (1982), where the C-terminal is believed to tilt away from the pore direction of a multimeric transmembrane channel. In fact, this picture also emerged from our optimization of the XRD structure to the solid-state NMR restrictions as visualized in Fig. 5 *A*. In the comparison of the XRD and MD structures, it should be noticed that they have almost identical overall tilt angles with respect to the bilayer normal, and that a 180° rotation of the wild-type MD structure around the average molecular axis (i.e., change of rotational pitch angle from ρ to $\rho + 180°$) leads to a structure that, to a good approximation, has interchanged tilts for the C- and N-terminal fragments in close agreement with the common XRD picture. Although, this orientation is characterized by a considerably higher RMSD value, it is quite obvious from the RMSD contour plot in Fig. 5 *C* that the traces through τ angles in the order of 5–15° are characterized by two "symmetry-related" minima with RMSD values of 5.1 and 12.1 for the τ, ρ values of 11°, 231° and 6°, 50°, respectively. It is relevant to note that, even with an XRD-inspired 180° rotation around the molecular axis, the wild-type MD structure remains in better agreement with the solid-state NMR data than does the XRD structure.

The solid-state NMR restrictions and their compatibility with various model structures may provide interesting new elements to the extensive discussion of alamethicin, its membrane-associated conformation, and its potential for multimerization and channel formation in the nonconductive state, which may have consequences also for the operation in the conductive state. From the solid-state NMR results, it can be concluded unambiguously that, for the present peptide:lipid ratio and hydration conditions, the vast majority of the alamethicin molecules are in a transmembrane configuration already in its nonconductive state. Thus, we find no compatibility with the large number of models where alamethicin in the nonconductive state forms monomeric or multimeric rods on the membrane surface (e.g., Baumann and Mueller, 1974; Banerjee et al., 1985; Biggin et al., 1997) or a bent structure with the C-terminal part on the membrane surface and the N-terminal extending into the membrane (e.g., Fox and Richards, 1982; Franklin et al., 1994). In turn, this implies that it is unlikely that

straightening-out of a kink about Pro^{14} or a flip of barrels from in-plane to transmembrane configuration is a major step in the activation of the pore upon introduction of a transmembrane potential. We note that the situation may be different at low peptide concentration (Tieleman, 1999a). Obviously, in contrast, our results support the various "barrel-stave" models with alamethicin oriented in a transmembrane fashion in both the nonconductive and the conductive state (e.g., Huang and Wu, 1991; North et al., 1995; Barranger-Mathys and Cafiso, 1996; Breed et al., 1997; Jayasinghe et al., 1998; Tieleman et al., 1999b,c). In particular, it should be noted that our results in this respect extend the conclusions arrived at by North et al. (1995) in their solid-state NMR analysis of the N-terminal part of the peptide to cover the full peptide.

Our results provide, for the first time, considerable experimental evidence that the most favorable orientation of alamethicin in phospholipid bilayers (specifically fully hydrated DMPC) is tilted by 10–20° relative to the bilayer normal, whereas nontilted conformations did not match the solid-state NMR restrictions. This should be seen in the light of previous solid-state NMR (North et al., 1995) and EPR (Barranger-Mathys and Cafiso, 1996; Jayasinghe et al., 1998) studies from which it was concluded that alamethicin is oriented parallel to the bilayer normal, but more recent model calculations appear to support a tilt in the order observed in this study (Kessel et al., 2000). In this regard, it should be emphasized that a tilted configuration would by no means be a surprise, considering the large number of tilted helix arrangements described for transmembrane helices (Bowie, 1997; Bywater et al., 2001). For example, tilted transmembrane helices have recently been determined experimentally for rhodopsin (Unger et al., 1997; Teller et al., 2001), the M2 channel of influenza A virus (Kovacs and Cross, 1997; Kukol et al., 1999), the epidermal growth factor receptor (Jones et al., 1998), the membrane protein Vpu from HIV-1 (Marassi et al., 1999), and the nicotinic acetylcholine receptor (Opella et al., 1999). Using numerical optimization, we found reasonable compatibility between the solid-state NMR restrictions and a straight α-helix tilting by 17° relative to the bilayer normal and a slightly bent MD structure with an overall tilt angle of 11°. Both angles are well within the typical regime of tilt angles for membrane-spanning helices. On the basis of the low number of NMR constraints, however, it is impossible to unambiguously prefer one or the other of these two possible solutions. We find compatibility with both structures and this cannot exclude the potential for a slightly bent structure in the membrane as has been proposed earlier (Barranger-Mathys and Cafiso, 1996). In this context, we note that recent MD calculations find evidence for a kink or at least dynamic hinge bending within the Gly^{11}-X-X-Pro^{14} motif, which may be important for the peptide to be able to accommodate relative motion of the two leaflets of the bilayer (Tieleman et al., 1999b,c). We note that the slightly kinked wild-type MD structure, in many respects, bears resemblance to the XRD structure (Fox and Richards, 1982), which, however, displayed a poorer match to our solid-state NMR restrictions.

There may be several not yet fully resolved reasons why alamethicin adopts a tilted orientation in the bilayer in the nonconductive state. First, several alamethicin monomers may, in the nonconductive state, form a preaggreate where a tilted conformation is favorable for the multimerization generally regarded necessary for the ion channel activity in the conductive state. Second, as an alternative, the monomers may adopt this orientation by themselves facilitating multimerization upon introduction of a transmembrane potential. Furthermore, if all helices are perpendicular to the membrane, it means that the helix–helix crossing angles will be 0° (or 180° if they are aligned counter-parallel). This is a very unfavorable crossing angle for helices (Bywater et al., 2001). With a nonperpendicular tilt angle, it is possible to construct multimeric aggregates with allowed crossing angles. Third, alamethicin may be monomeric (although it may be unlikely at the present high peptide:lipid ratio of 1:8), with a tilted conformation being energetically favorable because it provides optimum hydrophobic matching between the hydrophobic region of the peptide and the hydrocarbon region of the bilayers. The conformation may also prevent the side chains of both the C- or the N-terminal amino acids from moving in and out of hydrophobic or hydrophilic environments upon rotation of the peptide around the molecular axis (Jones et al., 1998). We note that our measurements do not allow for direct discrimination between monomeric and multimeric structures of alamethicin.

Among the three possible reasons for a tilted conformation of alamethicin in lipid bilayers, the two monomeric models do not require further discussion with respect to the solid-state NMR restrictions. In contrast, it appears reasonable to investigate how the solid-state NMR-compatible structures would fit into a multimeric model for alamethicin in the nonconductive state. In this context, we should mention that several models have been presented in the literature, which describe the conductive alamethicin channel as a pore lined by a bundle of approximately parallel α-helices (You et al., 1996; He et al., 1996a; Breed et al., 1997; Tieleman et al., 1999c). In general, these models accept different numbers of helices in the bundle, explaining the multiconductance behavior of the active alamethicin channel. Seen in this perspective, it would be interesting if the solid-state NMR compatible structures for alamethicin would allow for formation of, or describe the presence of, a multimeric bundle with the hydrofilic residues lining the pore of the channel. That this is indeed possible is demonstrated in Fig. 8, containing representative 6-mer alamethicin channels formed by symmetric packing of six differently rotated (around the bilayer normal) variants of the tilted α-helix and tilted/kinked wild-type MD structures from Fig.

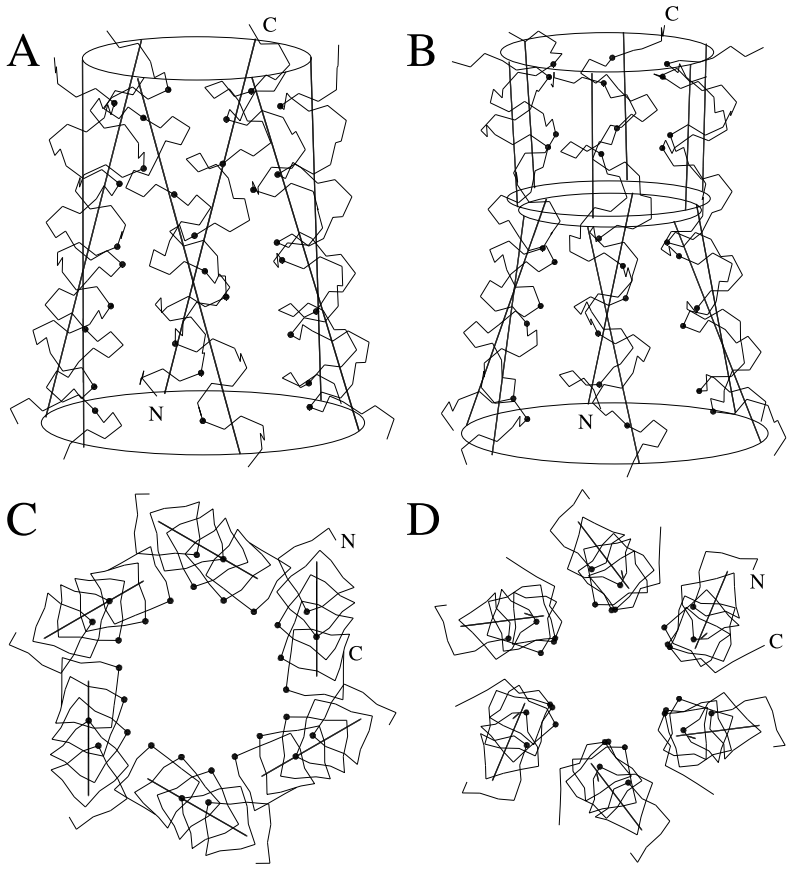

FIGURE 8 Models of hexameric alamathicin ion-channels generated from the (*A*) tilted α-helix (Fig. 5 *B*) and (*B*) tilted and kinked 100-ps wild-type MD structures (Fig. 5 *D*) being compatible with the solid-state NMR restrictions. The putative hexameric alamethicin channels are viewed from the side (*top*) and down the pore from the C-terminal end. The channels were constructed from monomers oriented relative to the bilayer as in Fig. 5 (parameters in Table 2) with the monomers rotated around the channel (i.e., bilayer normal) axis to optimize the hydrophilic character toward the channel core. We note that no attempts have been made to optimize the interactions between the monomers.

5, *B* and *D*, respectively. Although these multimeric packing motifs have been established without any attempts to model the interhelical spacing or specific sidechain interactions, it appears intuitively that the helices in a parallel arrangement for both models (independent of the number of participating helices) need to be packed as a left-handed bundle to ensure the hydrophilic lining in the interior of the channel. Furthermore, it should be noted that the observation of a single resonance in the solid-state NMR spectra for each labeled residue requires that all monomers participating in these putative channels are oriented identically with respect to the bilayer normal.

The use of the Varian XL-300 and Varian UNITY-INOVA 400 NMR spectrometers, sponsored by Teknologistyrelsen and the Danish Natural Science Foundation, at the University of Aarhus Instrument Centre for Solid-State NMR Spectroscopy is acknowledged. This research was in part supported by the Danish Natural Science Research Council (J.No. 9901954), Carlsbergfondet, the European Commission (BIO4-CT97-2101), and the FØTEK progamme (Danish Dairy board and the Danish Government). We thank P. Daugaard for assistance with construction of the flat-coil NMR probes and Dr. G. Vriend for providing us the WHAT IF program.

REFERENCES

Bak, M., J. T. Rasmussen, and N. C. Nielsen. 2000. SIMPSON: a general simulation program for solid-state NMR spectroscopy. *J. Magn. Reson.* 147:296–330. Laboratory for Biomolecular NMR, Department of Molecular and Structural Biology, University of Aarhus, Aarhus, Denmark. http://nmr.imsb.au.dk.

Ballesteros, J. A., and H. Weinstein. 1992. Analysis and refinement criteria for predicting the structure and relative orientations of transmembranal helical domains. *Biophys. J.* 62:107–109.

Banerjee, U., F. P. Tsui, T. M. Balasubramanian, G. R. Marshall, and S. I. Chan. 1983. Structure of alamethicin in solution. One- and two-dimensional ^{1}H nuclear magnetic resonance studies at 500 MHz. *J. Mol. Biol.* 165:757–775.

Banerjee, U., R. Zidovetzki, R. R. Birge, and S. I. Chan. 1985. Interaction of alamethicin with lecithin bilayers: ^{31}P and ^{2}H NMR study. *Biochemistry.* 24:7621–7627.

Bard, V. 1974. Nonlinear Parameter Estimation. Academic Press. New York.

Barlow, D. J., and J. M. Thornton. 1988. Helix geometry in proteins. *J. Mol. Biol.* 201:601–619.

Barranger-Mathys, M., and D. S. Cafiso. 1994. Collisions between helical peptides in membranes monitored using electron paramagnetic resonance: evidence that alamethicin is monomeric in the absence of a membrane potential. *Biophys. J.* 67:172–176.

Barranger-Mathys, M., and D. S. Cafiso. 1996. Membrane structure of voltage-gated channel forming peptides by site-directed spin-labeling. *Biochemistry.* 35:498–505.

Baumann, G., and P. Mueller. 1974. A molecular model of membrane excitability. *J. Supramolec. Struct.* 2:538–557.

Bechinger, B., Y. Kim, L. E. Chirlian, J. Gesell, J.-M. Neumann, M. Montal, J. Tomich, M. Zasloff, and S. J. Opella. 1991. Orientations of amphipathic helical peptides in membrane bilayers determined by solid-state NMR spectroscopy. *J. Biomol. NMR.* 1:167–173.

Bechinger, B., M. Zasloff, and S. J. Opella. 1993. Structure and orientation of the antibiotic peptide magainin in membranes by solid-state nuclear magnetic resonance spectroscopy. *Protein Sci.* 2:2077–2084.

Biggin, P. C., J. Breed, H. S. Son, and M. S. Sansom. 1997. Simulation studies of alamethicin–bilayer interactions. *Biophys. J.* 72:627–636.

Bowie, J. U. 1997. Helix packing in membrane proteins. *J. Mol. Biol.* 272:780–789.

Brachais, L., C. Mayer, D. Davoust, and G. Molle. 1998. Influence of the secondary structure on the pore forming properties of synthetic alamethicin analogs: NMR and molecular modelling studies. *J. Pept. Sci.* 4:344–354.

Brandl, C. J., and C. M. Deber. 1986. Hypothesis about the function of membrane-buried proline residues in transport proteins. *Proc. Natl. Acad. Sci. U.S.A.* 83:917–921.

Breed, J., I. D. Kerr, G. Molle, H. Duclohier, and M. S. Sansom. 1997. Ion channel stability and hydrogen bonding. Molecular modelling of channels formed by synthetic alamethicin analogues. *Biochim. Biophys. Acta.* 1330:103–109.

Burum, D. P., M. Linder, and R. R. Ernst. 1981. Low-power multipulse line narrowing in solid-state NMR. *J. Magn. Reson.* 44:173–188.

Burnett, M. N. and C. K. Johnson. 1996. Oak Ridge thermal ellipsoid plot program for crystal structure illustrations. Oak Ridge National Laboratory Report ORNL-6895.

Bywater, R. P., D. Thomas, and G. Vriend. 2001. A sequence and structural study of transmembrane helices. *J. Comp.-Aided Mol. Design*. 15: 533–552; and references cited herein.

Cafiso, D. 1994. Alamethicin: a peptide model for voltage gating and protein–membrane interactions. *Annu. Rev. Biophys. Biomol. Struct.* 23:141–165.

Chandrasekhar, K., M. K. Das, A. Kumar, and P. Balaram. 1988. Molecular conformation of alamethicin in dimethylsulfoxide solution: a two-dimensional NMR study. *Int. J. Peptide Protein Res.* 32:167–174.

Dathe, M., C. Kaduk, E. Tachikawa, M. F. Melzig, H. Wenschuh, and M. Bienert. 1998. Proline at position 14 of alamethicin is essential for hemolytic activity, catecholamine secretion from chromaffin cells and enhanced metabolic activity in endothelial cells. *Biochim. Biophys. Acta.* 1370:175–183.

Deber, C. M., M. Glibowicka, and G. A. Woolley. 1990. Conformations of proline residues in membrane environments. *Biopolymers*. 29:149–157.

Esposito, G., J. A. Carver, J. Boyd, and I. D. Campbell. 1987. High-resolution ^{1}H NMR study of the solution structure of alamethicin. *Biochemistry.* 26:1043–1050.

Fox, R. O., Jr., and F. M. Richards. 1982. A voltage-gated ion channel model inferred from the crystal structure of alamethicin at 1.5-Å resolution. *Nature.* 300:325–330.

Franklin, J. C., J. F. Ellena, S. Jayasinghe, L. P. Kelsh, and D. S. Cafiso. 1994. Structure of micelle-associated alamethicin from ^{1}H NMR. Evidence for conformational heterogeneity in a voltage-gated peptide. *Biochemistry.* 33:4036–4045.

Gibbs, N., R. B. Sessions, P. B. Williams, and C. E. Dempsey. 1997. Helix bending in alamethicin: molecular dynamics simulations and amide hydrogen exchange in methanol. *Biophys. J.* 72:2490–2495.

Harbison, G. S., L. W. Jelinski, R. E. Stark, D. A. Torchia, J. Herzfeld, and R. G. Griffin. 1984. ^{15}N Chemical shift and ^{15}N–^{13}C dipolar tensors for the peptide bond in [1-^{13}C]glycyl[^{15}N]glycine hydrochloride monohydrate. *J. Magn. Reson.* 60:79–82.

Harroun, T. A., W. T. Heller, T. M. Weiss, L. Yang, and H. W. Huang. 2000. Theoretical analysis of hydrophobic matching and membrane-mediated interactions in lipid bilayers containing gramicidin. *Biophys. J.* 76:3176–3185.

Hartzell, C. J., M. Whitfield, T. G. Oas, and G. P. Drobny. 1987. Determination of the ^{15}N and ^{13}C chemical shift tensors of L-[^{13}C]alanyl-L-[^{15}N] alanine from the dipole-coupled powder patterns. *J. Am. Chem. Soc.* 109:5966–5969.

He, K., S. J. Ludtke, D. L. Worcester, and H. W. Huang. 1996a. Neutron scattering in the plane of membranes: structure of alamethicin pores. *Biophys. J.* 70:2659–2666.

He, K., S. J. Ludtke, W. T. Heller, and H. W. Huang. 1996b. Mechanism of alamethicin insertion into lipid bilayers. *Biophys. J.* 71:2669–2679.

Hester, R. K., J. L. Ackerman, V. R. Cross, and J. S. Waugh. 1975. Resolved dipolar coupling spectra of dilute nuclear spins in solids. *Phys. Rev. Lett.* 34:993–995.

Huang, H. W., and Y. Wu. 1991. Lipid-alamethicin interactions influence alamethicin orientation. *Biophys. J.* 60:1079–1087.

Jacob, J., H. Duclohier, and D. S. Cafiso. 1999. The role of proline and glycine in determining the backbone flexibility of a channel-forming peptide. *Biophys. J.* 76:1367–1376.

Jaikaran, D. C., P. C. Biggin, H. Wenschuh, M. S. Sansom, and G. A. Woolley. 1997. Structure–function relationships in helix-bundle channels probed via total chemical synthesis of alamethicin dimers: effects of a Gln^{7} to Asn^{7} mutation. *Biochemistry.* 36:13873–13881.

Jayasinghe, S., M. Barranger-Mathys, J. F. Ellena, C. Franklin, and D. S. Cafiso. 1998. Structural features that modulate the transmembrane migration of a hydrophobic peptide in lipid vesicles. *Biophys. J.* 74: 3023–3030.

Jones, D. H., K. R. Barber, E. W. VanDerLoo, and C. W. M. Grant. 1998. Epidermal growth factor receptor transmembrane domain: ^{2}H NMR implications for orientation and motion in bilayer environment. *Biochemistry.* 37:16780–16787.

Kabsch, W., and C. Sander. 1983. Dictionary of protein secondary structure: pattern recognition of hydrogen bond and geometrical features. *Biopolymers.* 22:2577–2637.

Kelsh, L. P., J. F. Ellena, and D. S. Cafiso. 1992. Determination of the molecular dynamics of alamethicin using ^{13}C NMR: implications for the mechanism of gating of a voltage-dependent channel. *Biochemistry.* 31:5136–5144.

Ketchem, R. R., W. Hu, and T. A. Cross. 1993. High-resolution conformation of gramicidin A in a lipid bilayer by solid-state NMR. *Science.* 261:1457–1460.

Kessel, A., D. S. Cafiso, and N. Ben-Tal. 2000. Continuum solvent model calculations of alamethicin–membrane interactions: thermodynamic aspects. *Biophys. J.* 78:571–583.

Kovacs, F. A., and T. A. Cross. 1997. Transmembrane four-helix bundle of influenza A M2 protein channel: structural implications from helix tilt and orientation. *Biophys. J.* 73:2511–2517.

Kovacs, F. A., J. K. Denny, Z. Song, J. R. Quine, and T. A. Cross. 2000. Helix tilt of the M2 transmembrane peptide from influenza A virus: an intrinsic property. *J. Mol. Biol.* 295:117–125.

Kukol, A., P. D. Adams, L. M. Rice, A. T. Brunger, and I. T. Arkin. 1999. Experimentally based orientational refinement of membrane protein models: a structure for the influenza A M2 H^{+} channel. *J. Mol. Biol.* 286:951–962.

Levy, S., T. Munzner, M. Phillips, and others. 1996. Geomview 1.6.1, The Geometry Center, University of Minnesota, Minneapolis, http://www.geomview.org/.

Lewis, B. A., and D. M. Engelman. 1983. Lipid bilayer thickness varies linearly with acyl chain length in fluid phosphatidylcholine vesicles. *J. Mol. Biol.* 166:211–217.

Mai, W., W. Hu, C. Wang, and T. A. Cross. 1993. Orientational constraints as three-dimensional structural constraints from chemical shift anisotropy: the polypeptide backbone of gramicidin A in a lipid bilayer. *Protein Sci.* 2:532–542.

Marassi, F. M., C. Ma, H. Gratkowski, S. K. Straus, K. Strebel, M. Oblatt-Montal, and S. J. Opella. 1999. Correlation of the structural and functional domains in the membrane protein Vpu from HIV-1. *Proc. Natl. Acad. Sci. U.S.A.* 96:14336–14341.

Mohamadi, F., N. G. J. Richards, W. C. Guida, R. Liskamp, M. Lipton, C. Caufield, T. Hendrickson, and C. Still. 1990. MacroModel—an integrated software system for modeling organic and bioorganic molecules using molecular mechanics. *J. Comput. Chem.* 11:440–467.

Nielsen, N. C., P. Daugaard, V. Langer, J. K. Thomsen, S. Nielsen, O. W. Sørensen, and H. J. Jakobsen. 1995. A flat-coil NMR probe with hydration control of oriented phospholipid bilayer samples. *J. Biomol. NMR.* 5:311–314.

Nilsson, I., A. Sääf, P. Whitley, G. Gafvelin, C. Walther, and G. von Heijne. 1998. Proline-induced disruption of a transmembrane α-helix in its natural environment. *J. Mol. Biol.* 284:1165–1175.

North, C. L., M. Barranger-Mathys, and D. S. Cafiso. 1995. Membrane orientation of the N-terminal segment of alamethicin determined by solid-state ^{15}N NMR. *Biophys. J.* 69:2392–2397.

Oas, T. G., C. J. Hartzell, F. W. Dahlquist, and G. P. Drobny. 1987. The amide ^{15}N chemical shift tensors of four peptides determined from ^{13}C dipole-coupled chemical shift powder patterns. *J. Am. Chem. Soc.* 109: 5962–5966.

Opella, S. J., P. L. Stewart, and K. G. Valentine. 1987. Protein structure by solid-state NMR spectroscopy. *Quatr. Rev. Biophys.* 19:7–49.

Opella, S. J., F. M. Marassi, J. J. Gesell, A. P. Valente, Y. Kim, M. Oblatt-Montal, and M. Montal. 1999. Structures of the M2 channel-lining segments from nicotinic acetylcholine and NMDA receptors by NMR spectroscopy. *Nature Struct. Biol.* 6:374–379.

Pandey, R. C., J. C. Cook, and K. L. Rinehardt, Jr. 1977. High resolution and field desorption mass spectrometry studies of revised structures of alamethicins I and II. *J. Am. Chem. Soc.* 99:8469–8483.

Peersen, O. B., S. Yoshimura, H. Hojo, S. Aimoto, and S. O. Smith. 1992. Rotational resonance NMR measurements of internuclear distances in an alpha-helix peptide. *J. Am. Chem. Soc.* 114:4332–4335.

Piela, L., G. Nemethy, and H. A. Scheraga. 1987. Proline-induced constraints in alpha-helices. *Biopolymers.* 26:1587–1600.

Pines, A., M. G. Gibby, and J. S. Waugh. 1973. Proton-enhanced NMR of dilute spins in solids. *J. Chem. Phys.* 59:569–590.

Ramamoorthy, A., F. M. Marassi, M. Zasloff, and S. J. Opella. 1995. Three-dimensional solid-state NMR spectroscopy of a peptide oriented in membrane bilayers. *J. Biomol. NMR.* 6:329–334.

Sanson, M. S. P. 1993. Structure and function of channel-forming peptaibols. *Q. Rev. Biophys.* 26:365–421.

Schwarz, G. S., S. Stankowski, and V. Rizzo. 1986. Thermodynamic analysis of incorporation and aggregation in a membrane: application to the pore-forming peptide alamethicin. *Biochem. Biophys. Acta.* 861: 141–151.

Scherer, J. P. 1989. On the position of the hydrophobic/hydrophilic boundary in lipid bilayer. *Biophys. J.* 55:957–964.

Sessions, R. B., N. Gibbs, and C. E. Dempsey. 1998. Hydrogen bonding in helical polypeptides from molecular dynamics simulations and amide hydrogen exchange analysis: alamethicin and melittin in methanol. *Biophys. J.* 74:138–152.

Shoji, A., S. Ando, S. Kuroki, I. Ando, and G. A. Webb. 1993. Structural studies of peptides and polypeptides in the solid state by nitrogen-15 NMR. *Ann. Rep. NMR Spectrosc.* 26:55–98.

Teller, D. G., T. Okada, C. A. Behnke, K. Palczewski, and R. E. Stenkamp. 2001. Advances in determination of a high-resolution three-dimensional structure of rhodopsin, a model of g-protein-coupled receptors (gpcrs). *Biochemistry.* 40:7761–7772.

Teng, Q., and T. A. Cross. 1989. The in situ determination of the ^{15}N chemical-shift tensor orientation in a polypeptide. *J. Magn. Reson.* 85:439–447.

Tieleman, D. P., J. C. Berendsen, and M. S. P. Sansom. 1999a. Surface binding of alamethicin stabilizes its helical structure: molecular dynamics simulations. *Biophys. J.* 76:3186–3191.

Tieleman, D. P., M. S. P. Sansom, and J. C. Berendsen. 1999b. Alamethicin helices in a bilayer and in solution: molecular dynamics simulations. *Biophys. J.* 76:40–49.

Tieleman, D. P., J. C. Berendsen, and M. S. P. Sansom. 1999c. An alamethicin channel in a lipid bilayer: molecular dynamics simulations. *Biophys. J.* 76:1757–1769.

Unger, V. M., P. A. Hargrave, J. M. Baldwin, and G. F. X. Schertler. 1997. Arrangement of rhodopsin transmembrane α-helices. *Nature.* 389: 203–206.

von Heijne, G. 1991. Proline kinks in α-helices. *J. Mol. Biol.* 218:499–503.

Vriend, G. 1990. WHAT IF: a molecular modelling and drug design program. *J. Mol. Graph.* 8:52–56.

Woolley, G. A., and B. A. Wallace. 1993. Temperature dependence of the interaction of alamethicin helices in membranes. *Biochemistry.* 32: 9819–9825.

Wu, Y., H. W. Huang, and G. A. Olah. 1990. Method of oriented circular dichroism. *Biophys. J.* 57:797–806.

Wu, C. H., A. Ramamoorthy, and S. J. Opella. 1994. High-resolution heteronuclear dipolar solid-state NMR spectroscopy. *J. Magn. Reson. A.* 109:270–272.

Wu, C. H., A. Ramamoorthy, L. M. Gierasch, and S. J. Opella. 1995. Simultaneous characterization of the amide ^{1}H-chemical shift, ^{1}H–^{15}N dipolar, and ^{15}N chemical shift interaction tensors in a peptide bond by three-dimensional solid-state NMR spectroscopy. *J. Am. Chem. Soc.* 117:6148–6149.

Yee, A. A., and D. J. O'Neil. 1992. Uniform ^{15}N labeling of a fungal peptide: the structure and dynamics of an alamethicin by ^{15}N and ^{1}H NMR spectroscopy. *Biochemistry.* 31:3135–3143.

Yee, A. A., K. Marat, and J. D. O'Neil. 1997. The interactions with solvent, heat stability, and ^{13}C-labelling of alamethicin, an ion-channel-forming peptide. *Eur. J. Biochem.* 243:283–291.

You, S., S. Peng, L. Lien, J. Breed, M. S. P. Sansom, and G. A. Woolley. 1996. Engineering stabilized ion channels: covalent dimers of alamethicin. *Biochemistry.* 35:6225–6232.